An Augmented Reality Framework for Optimization of Computer Assisted Navigation in Endovascular Surgery

Irene Cheng, *IEEE Senior Member*, Rui Shen, Richard Moreau, Vicenzo Brizzi, Nathaniel Rossol and Anup Basu, *IEEE Senior Member*

Abstract— Endovascular surgery is performed by placing a catheter through blood vessels. Due to the fragility of arteries and the difficulty in controlling a long elastic wire to reach the target region, training plays an extremely important role in helping a surgeon acquire the required complex skills. Virtual reality simulators and augmented reality systems have proven to be effective in minimally invasive surgical training. These systems, however, often employ pre-captured or computer-generated medical images. We have developed an augmented reality system for ultrasound-guided endovascular surgical training, where real ultrasound images captured during the procedure are registered with a pre-scanned phantom model to give the operator a realistic experience. Our goal is to extend the planning and training environment to deliver a system for computer assisted remote endovascular surgery where the navigation of a catheter can be controlled through a robotic device based on the guidance provided by an endovascular surgeon.

I. Introduction

Endovascular surgery is a type of Minimally Invasive Surgery (MIS) designed to access target regions of the human body through blood vessels [1]. In recent years, technological advances in hardware and software have been achieved, resulting in higher procedural success [2]. While endovascular surgery is increasingly deployed to replace classical surgery for improving recovery time and patient safety, there are still challenges to sustain a safe environment for patients as well as doctors. Ongoing research aims at reducing surgery time, and minimizing exposure to radiation. Currently, medical personnel require heavy cumbersome protective clothing which, nevertheless, can cover only part of the body. Classical solutions based on wire-driven robots are proposed in the literature [3]. The main concern of a wire-driven catheter approach is the difficulty in identifying the friction and thus potential damage to the vessels. An alternative is to assemble several independent units in a serial configuration, but this increases design and operation complexity. In related research, Zhang et al. proposed endoscopes for fetal MIS with six degree-of-freedom [4] and to estimate the contact force by measuring the wire tension. Other solutions have been developed to offer more possibilities of controlling the endoscope tip [5, 6]. The main drawback of these techniques is the permanent contact exerted on the tube inside which the tip moves inducing potential danger to the blood vessels.

This research was supported by grants from NSERC and Alberta Innovates Technology Futures.

Irene Cheng, Rui Shen and Anup Basu are with the Department of Computing Science, University of Alberta, Edmonton, Canada. Emails: {locheng, rshen, nrossol, basu}@ualberta.ca.

Richard Moreau is with the Ampere Lab, INSA, Lyon, France. Email: rmoreau@insa-lyon.fr. Vicenzo Brizzi is with Bordeaux Regional Hospital. Email: vinbrizzi@hotmail.com.

Valuable studies have been expended to examine the effective control of catheters and active endoscopes [7, 8, 9]. The effect of stiffness for surgical manipulators is discussed by Mavash and Dupont [10]. Despite these efforts, lack of real-time interactive 3D visualization, and automatic planning, tracking and adjusting of a surgical end-effector, continue to motivate intensive research. The focus of this paper is on endovascular surgery and the related challenges. We introduce an augmented reality framework for optimization of computer assisted navigation in endovascular surgery. Our contributions lie in: (1) Developing an effective environment for endovascular planning, training and surgery. The design criteria aim at reducing surgical time and increasing safety. (2) Assisting surgeons plan optimal paths for catheter navigation and allow for corrective real-time adjustments during operation. (3) Providing 3D visualization mechanism for accurate tracking and diagnosis. (4) Performing accurate transformation to various coordinate systems and enabling robust registration of different data modalities.

The remainder of this paper is organized as follows: Section II reviews methods for blood vessel segmentation. Details of our framework are explained in Section III, before the work is concluded in Section IV.

II. Extraction of Blood Vessel and Medial Axis Using Our Segmentation Technique

During an endovascular procedure, a catheter is inserted into the blood vessels from the femoral. In a simulation or augmented reality environment, the successful navigation and bending of the catheter inside the vessels relies on the accuracy of the segmented models.

There is a variety of work on segmentation related to vascular structures. The broad problem of segmentation of tubular structures is addressed in the literature [11, 12]. Generalized cylinders are used by researchers for blood vessel segmentation [13]. Multi-attribute fuzzy clustering and spatial continuity are enforced in the blood vessel segmentation process [9]. However, these techniques are designed for specific data modalities. Due to the complexity of the artery hierarchy and the surrounding anatomical structures (Fig. 1 (b)), the outcomes of segmentation from these algorithms are unsatisfactory.

We enhanced 3D segmentation of blood vessels [14] by applying initialization of 2D livewires in two orthogonal directions, and extracted robust 3D medial axes for smooth surgical tool trajectory planning by using a new scale-space skeletonization algorithm. Since the intensities of arteries are close to the intensities of the bone structures in the dye-enhanced CT series (Fig. 1 (a)), simple window threshold techniques are insufficient for segmenting arteries. The

target region has to be scanned at the time when the dye has emerged in order to obtain good contrast images. We used a semi-automatic 3D segmentation environment employing 3D livewires [15]. The Livewires in three directions form a 'seed-point map' which is used to perform automatic 2D Livewire segmentation in other slices. Fig. 1 (c) illustrates the segmented artery using this method. The accuracy of the segmented 3D arteries is verified by clinical surgeons. A result of robust 3D medial axis extraction of blood vessels can be seen in Fig. 1 (d); details of the algorithm on this part are available in our earlier publications [16, 21]. Our approach can adaptively adjust the scale during skeletonization, thereby being able to keep track of both wide and narrow regions of a blood vessel.

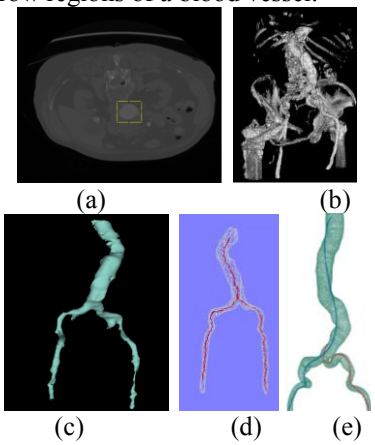

Fig. 1: (a) Sample low contrast CT slice in axial view with the aorta inside the rectangle; (b) artery neighborhood from OSIRIX after intensity windowing; (c) 3D segmentation using initialization of livewires followed by Turtleseg; (d) medial axis generated inside the artery 3D model; and (e) artery phantom: with optimal path chosen by surgeon for catheter navigation.

III. PROPOSED FRAMEWORK

The extracted 3D medial axis can only be used as a reference for the electromagnetic tracker. The ultimate path for navigating the surgical tool may deviate from the medial axis and has to be defined based on the artery capacity, muscle resistance and the surgeon's decision on the patient's status. Fig. 1 (e) illustrates a planned path for surgery. Note that it deviates from the medial axis and needs the support of the vessel wall in order to bend into the next artery segment.

There are two main considerations to ensure damage to the artery can be eliminated or minimized during the procedure: (1) the spot to bend the catheter around a curve, and (2) the resistance of the tissue at this spot taking into account the artery environment and external fixation. It is possible that there is calcification in arteries leading to loss of elastic properties and the artery becomes more fragile. By examining the CT scan, surgeons can identify calcium. We incorporate expert opinion in our computational model and assign appropriate resistance values on vessel segments. The fragility measurement can also be obtained by analyzing arterial walls [17]. Our novelty lies in integrating this information in the catheter navigation path planning process and providing real-time verification.

A. Path Computation Model

We define artery ϑ as a sequence of sub-segments, *i.e.*

$$\vartheta = \{s: 1 \leq s \leq S_{max}\} \quad (1)$$

where S_{max} is the total number of sub-segments along the artery that the catheter has to traverse. The number of sub-segments is governed by the geometry of the traversed path and can be computed based on the number of critical points explained below. The deviation of the planned navigation from the medial axis in a given sub-segment is computed as:

$$\emptyset_s = (\alpha_s cos(t), \beta_s sin(t)) \quad (2)$$

where $0 \leq t \leq 2\pi$. The radius of the blood vessel at that point is τ_s, *i.e.* $\alpha_s \leq \tau_s$ *and* $\beta_s \leq \tau_s$ are resistance values of the vessel in sub-segment *s* based on expert opinion. The parameter *t* controls the angular component of the path on the plane perpendicular to the medial axis. A bigger α_s or β_s value means bigger resistance and the catheter is safe to get closer to the vessel boundary. When there is no deviation from the medial axis, $\alpha_s = \beta_s = 0$. To define the navigation path in a given sub-segment, we use a 3D vector:

$$\overrightarrow{\rho_s} = (\alpha_s cos(t), \beta_s \sin(t), \gamma_s) \quad (3)$$

The 3rd parameter γ_s corresponds to the length of sub-segment *s*. Thus, the entire navigation path is denoted by:

$$\vec{C} = \sum_{s=1}^{S_{max}} \overrightarrow{\rho_s} \quad (4)$$

It can be seen that the computation model can simulate a navigation path within arteries similar to how a surgeon inserts a catheter manually. Fig. 2 shows an example of a navigation path deviating from the medial axis.

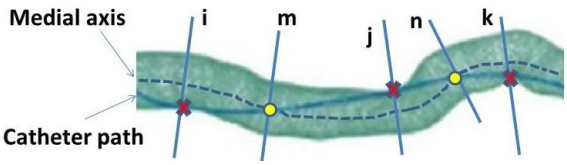

Fig. 2: The catheter has a navigation path different from the medial axis in order to turn around curves. Critical points are marked with "X"s. Intermediate points (circles) can be added to improve interpolation between critical points.

B. Navigation Path Planning

The locations where the path leans on the vessel are called critical points (marked with X in Fig. 2). They are extrema satisfying the Lapacian Equation $\nabla^2 C = 0$. The solid lines in Fig. 2 indicate the critical sub-segments *i*, *j* and *k*, while m and n denote intermediate points. The catheter wire relies on the support at critical points and bends towards the next desired direction. This is necessary to turn around curves or enter an artery side-branch. The path between critical points can be interpolated. Intermediate points, *e.g.,* marked with circles in Fig. 2, can be specified and are helpful to streamline the interpolated path. Points of inflection derived from the 2nd derivative are useful intermediate points. In general, defining more points delivers a smoother trajectory but the trade-off is adverse time performance especially in real-time applications.

We propose equal length sub-segments to facilitate processing. Thus, $\gamma_s = c$ where c is a constant and $c = min(\mathcal{D}, \Re)$. $\mathcal{D}$ is the shortest inter-point distance measured along the medial axis, and $\Re$ is the shortest distance along the medial axis reflecting a significant change in resistance.

C. Relative Resistance Look-up Table

t / s	1 …	i …	m …	J …	n …	k …	… S_{max}
0	0	1	0	1	0	1	:
	:	:	:	:	:	:	:
	0.3	:	0.2	0.2	:	:	:
	:	:	0.2	0.3	:	:	:
2π	0	:	:	:	:	:	:

Table 1: Relative resistance look-up table: Each row corresponds to S_{max} sub-segments along the navigation path and each column records the angular change in resistance.

The Visualization Component of our framework will display the planned path, as well as the medial axis, during the procedure. The optimal path is defined by the surgeons based on their expertise. To compare the relative resistance, a normalized scale from 0 to 1 is used. When the value is 0, the path follows the medial axis. A value of 1 indicates a critical point. Based on the planned path, a look-up table can be implemented as illustrated in Table 1 to support real-time performance. During the planning step, the surgeon can identify the critical points and assign appropriate scale values. The different scale values are mapped onto different gray scale colors and displayed along the medial axis so that the surgeon can visualize the predicted changes in resistance along the vessel. For simple resistance pattern with insignificant angular change, critical points are recorded only in 1D (*e.g.*, the first row in Table 1). However, the table is designed to support complex patterns like in sub-segment *1* and the four fragility values recorded in sub-segment *m* and *j*. In future work, it is possible, though challenging, to put an instrument at the top of a wire, and measure tissue fragility during real-time navigation based on all forces encountered and refine the planned optimal path if significant difference is detected. Updated resistance values can also be recorded in the table.

D. Augmented Reality & Navigation Visualization

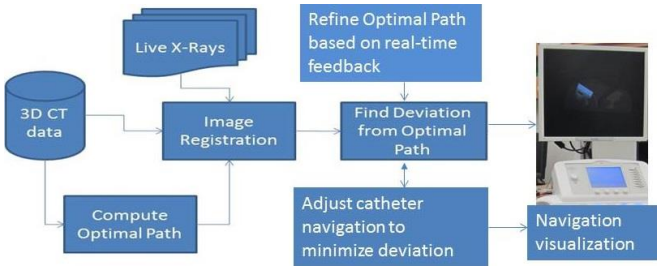

Fig. 3: An illustration of data registration, path computation and correction steps in our proposed framework.

Enhancement of endovascular procedures can come from 3D visualization (Fig. 3). Indeed, it can be used to allow surgeons to locate their tools inside a patient's body and to have position or force feedback. Our prototype implementation consists of an ultrasound machine, a phantom, and a visualization software module, as shown in Fig. 4. The system integrates ultrasound images of a phantom captured during surgical training with a digitized model of the phantom, and displays the integrated 3D scene to the user. In this way, the user can have a better understanding of the catheter's position in the phantom, and can then adjust the operation accordingly. The phantom is ultrasound compatible, and contains two vessels that can be used for placing a catheter during training. The phantom was pre-scanned to form a 3D digital model, which is used by the visualization module.

Fig. 4: Operation setup for our proposed framework.

E. Registration of coordinate systems

The ultrasound machine used in our training system contains a GPS tracking module [18]. Both the probe and the needle (i.e., the catheter tip) have built-in electromagnetic sensors, the positions of which can be picked up by the GPS tracking module. The position and orientation of a captured ultrasound image in the GPS coordinate system are recovered, and is used by the visualization module.

In order for an ultrasound image to be rendered in the correct position and orientation, relative to the 3D phantom model, the GPS coordinate system needs to be registered with the 3D phantom model's coordinate system. This registration requires two coordinate system transformations: the transformation between the GPS coordinate system and the world coordinate system (*i.e.*, the coordinate system of the space that the physical phantom resides in), and the transformation between the world coordinate system and the model coordinate system (*i.e.,* the coordinate system of the space that the virtual phantom resides in).

The transformations are estimated as follows. The phantom is placed at a pre-defined planar rectangular region. We define the world coordinate system based on this rectangular region, so that the model coordinate system coincides with the world coordinate system. The probe is placed at multiple known locations (at least three) in the rectangular region. For example, the probe can be placed at the four corners. Then, based on the rectangle's position and orientation in the GPS coordinate system, the transformation between the GPS coordinate system and the world/model coordinate system can be determined.

The ultrasound images, together with the GPS coordinates, are passed to the visualization module. Based on the estimated transformation, the ultrasound images are placed inside the 3D phantom model. This integrated 3D scene, together with the virtual medial axis and planned navigation path, are then rendered and displayed to the user.

F. Robotic Device Control

One of the issues in developing an active endoscopic type mechanism is the limited space available for the actuators. Also, without real-time visualization, it is impossible to assess and monitor the hardware performance. In contrast,

our hardware component is designed to smoothly integrate with the visualization component.

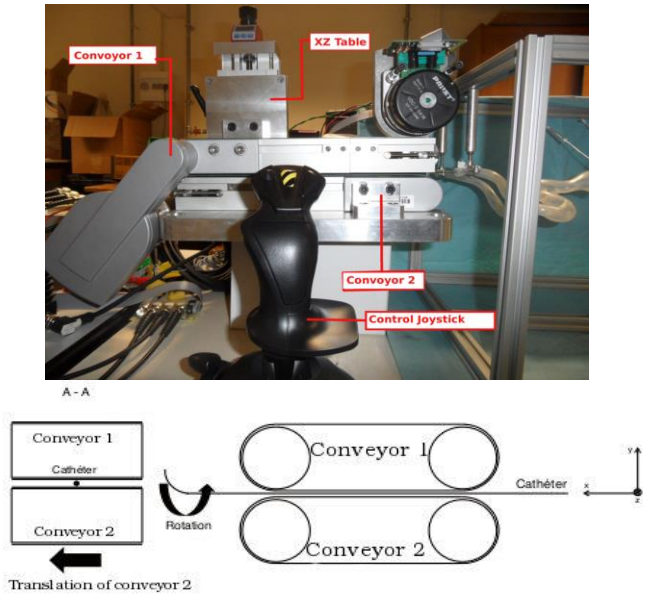

Fig. 5: Mechanical device for moving a catheter electronically.

Our prototype for the mechanical device is composed of two conveyors and a motorized XZ table (Fig. 5 top & middle). The guide wire and the catheter can be inserted between the two conveyors. The velocity of these conveyors is controlled via a joystick to ensure the longitudinal displacement of the guide wire. One of the conveyors is fixed whereas the second one is mounted on the XZ table. The displacement of the XZ table allows translation of one conveyor and thus rotates the guide wire, which is also controlled via the same joystick. Fig. 5 (bottom) shows the control device (left), moving the catheter into the artery phantom (right).

IV. Discussion and Conclusion

Due to the complexity of endovascular procedures, training plays a crucial role in assisting a surgeon acquires the necessary skills. Virtual reality simulators, which employ real-world information and virtual digital content, have proven to be effective in surgical training [19, 20]. Motivated by the application requirements, we propose an augmented reality system for ultrasound and electro-magnetic tracking guided endovascular surgical training, where real ultrasound images captured during the training are registered with a pre-scanned phantom model to give the user visual feedback and a more realistic experience. The novelty of the proposed system lies in the capability of allowing surgeons to pre-plan an optimal path with tissue resistance information. The navigation path can be adjusted during operation based on real-time feedbacks. Our mechanical device virtually converts the surgical tool into an "intelligent wire" and eases the difficulties encountered in navigation. Currently, the visualization interface provides basic interaction functionalities, such as pan, zoom, and rotation, which can be accessed through a mouse or a keyboard. In future work, we will integrate gesture and voice commands to control the visualization interface, which will give the user more flexibility when using our system. We will also look into the clinical safety aspect before releasing the system beyond training.

References

[1] Guo, S., Kondo, H., Wang, J., Guo, J., Tamiya, T., "A New Catheter Operating System for Medical Applications," Proc. IEEE Int. Conf. Complex Medical Engineering, Beijing, China, 82-86 (2007).

[2] L.W. Klein et al., "The catheterization laboratory and interventional vascular suite of the future: Anticipating innovations in design and function," Catheter Cardiovasc Interv., 77, 447-455 (2011).

[3] G.A. Antoniou et al., "Clinical applications of robotic technology in vascular and endovascular surgery," J. vascular surgery, Feb 2011, vol. 53, no. 2, 493-499 (2011).

[4] B. Zhang et al., "Development of 6-DOF wire-driven robotic manipulator for minimally invasive fetal surgery," Proc. IEEE Int. Conf. Robotics and Automation, Shanghai, China, 2892-2897 (2011).

[5] Bailly, Y. and Amirat, Y., "Modeling and Control of a Hybrid Continuum Active Catheter for Aortic Aneurysm Treatment," Proc. IEEE Int. Conf. Robotics and Automation, Barcelona, Spain, 924-929 (2005).

[6] V. Mangnan et al., "Development of a peristaltic endoscope," Proc. IEEE Int. Conf. Robotics and Automation, Washington, 347–352, 2002.

[7] V. De Sars et al., "A practical approach to the design and control of active endoscopes," Mechatronics, 20:2, 251-264 (2009).

[8] Simi, M., Sardi, G., Valdastri, P., Menciassi, A., and Dario, P., "Magnetic Levitation Camera Robot for Endoscopic Surgery," Proc. IEEE Int. Conf. Robotics and Automation, Shanghai, China, 5279-5284 (2011).

[9] Hao, J., Zhao, J. and Li, M., "Spatial continuity incorporated multi-attribute fuzzy clustering algorithm for blood vessels segmentation," SCIENCE CHINA Information Sciences, 53, 752-759 (2010).

[10] Mahvash, M. and Dupont, P., "Stiffness Control of Surgical Manipulators," IEEE Trans. Robotics, 27:2, 334-345 (2011).

[11] Benmansour, F. and Cohen, L., "Tubular Structure Segmentation Based on Minimal Path Method and Anisotropic Enhancement," J. Computer Vision, Springer Netherlands, *92*, 192-210 (2011).

[12] Kirbas, C. and Quek, F., "A review of vessel extraction techniques and algorithms," ACM Comput. Surv., 36, 81-121 (2004).

[13] L. Flórez Valencia et al. *(Eds.),* "Algorithm for Blood-Vessel Segmentation in 3D Images Based on a Right Generalized Cylinder Model: Application to Carotid Arteries," Computer Vision and Graphics, Springer Berlin / Heidelberg, 6374, 27-34 (2010**).**

[14] A. G. Radaelli and J. Peiró, On the segmentation of vascular geometries from medical images, *Int. Journal for Numerical Methods in Biomedical Engineering,* 3-34, 2010.

[15] M. Poon, G. Hamameh and R. Abugharbieh, Efficient interactive 3D Livewire segmentation of objects with arbitrarily topologies, *Comp. Medical Imaging and Graphics,* 2008.

[16] L. Shi, I. Cheng and A. Basu, Anatomy preserving 3D model decomposition based on robust skeleton-surface node correspondence, *Int. Conf. on Multimedia & Expo,* 6 pages, 2011.

[17] Aortic endovascular repair modeling using the finite element method, J. Biomedical Science and Engineering 2013, 6, 917-927, Mouktadiri G., Bou-Saiid B. and Walter-Le-Berre H.

[18] J. D. Hoelscher, Development of a Robust, Accurate Ultrasonic Tracking System for Image Guided Surgery, MS Thesis, *Southern Illinois University Carbondale*, 2008.

[19] R. Aggarwal et al., "Virtual Reality Simulation Training can Improve Inexperienced Surgeons' Endovascular Skills," In *European Journal of Vascular and Endovascular Surgery*, vol. 31, no. 6, 588–593.

[20] P. Lamata et al., "Augmented Reality for Minimally Invasive Surgery: Overview and Some Recent Advances," In *Augmented Reality*, 73–98.

[21**]** I. Cheng, A. Firouzmanesh, A. Leleve, R. Shen, R. Moreau, V. Brizzi, M.-T. Pham, P. Lermusiaux, T. Redarce, A. Basu, "Enhanced Segmentation and Skeletonization for Endovascular Surgical Planning," 7 pages, SPIE Medical Imaging, San Diego, February 2012.